

1 EXTENSIVE STUDY OF THE POSITIVE AND NEGATIVE PARITY  
2 WOBBLING STATES FOR AN ODD-MASS TRIAXIAL NUCLEUS II:  
3 CLASSICAL TRAJECTORIES

4 R. POENARU<sup>1,2,a</sup>, A. A. RADUTA<sup>2,3,b</sup>

5 <sup>1</sup>Doctoral School of Physics, University of Bucharest, Bucharest, Romania

6 *E-mail<sup>a</sup>*: robert.poenaru@drd.unibuc.ro

7 <sup>2</sup>Department of Theoretical Physics - Horia Hulubei National Institute for Physics and Nuclear  
8 Engineering, Măgurele-Bucharest, Romania

9 *E-mail<sup>b</sup>*: raduta@nipne.ro (corresponding author)

10 <sup>3</sup>Academy of Romanian Scientists, Bucharest, Romania

11 Received: April 21, 2021 (RJP v2.0 r2018a)

12 *Abstract.* **To be implemented...**

13 *Key words:* Triaxial Nuclei, Wobbling Motion, Angular Momentum, Energy El-  
lipsoid.

1. INTRODUCTION

14 Collective phenomena in deformed nuclei such as the *wobbling motion* have  
15 been drawing a lot of attention lately, mainly due to its elusive character, but also  
16 due to the real experimental and theoretical challenges it implies. Considered as a  
17 clear fingerprint of nuclear triaxiality, wobbling motion (w.m.) has been predicted  
18 theoretically by Bohr and Mottelson more than 40 years ago [1], when they were  
19 discussing the excited spectra of even-even nuclei using a triaxial rigid rotor with  
20 three different moments of inertia (MOI).

21 W.m. can be viewed as the quantum analogue for the motion of the asymmet-  
22 ric top, whose rotation around the axis with the largest moment of inertia (MOI) is  
23 energetically the most favored. A uniform rotation about this axis will have the low-  
24 est energy for a given angular momentum (spin). As the energy increases, this axis  
25 will start to precess, due to the anisotropy of the three moments of inertia, with a  
26 harmonic type of oscillation about the space-fixed angular momentum vector, giving  
27 rise to a family of wobbling bands, each characterized by a wobbling phonon num-  
28 ber  $n_w$ . The resulting quantal spectrum will be a sequence of  $\Delta I = 2\hbar$  rotational  
29 bands, with an alternating signature number ( $\alpha = \pm \frac{1}{2}$  in odd- $A$  nuclei and  $\alpha = 0, 1$   
30 in even- $A$  nuclei) for each wobbling excitation.

31 Although Bohr and Mottelson made predictions for these excitations in even-  
32 even nuclei, the first experimental evidence of this nuclear behavior has been identi-  
33 fied in an odd-mass nucleus: the  $A = 163$  isotope of Lu, where a single one-phonon

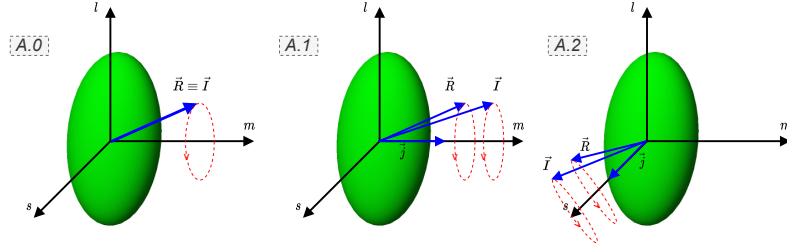


Fig. 1 – A.0: The geometry for the angular momentum of a simple wobbler. A.1: coupling geometry for a longitudinal wobbler (LW). A.2: coupling geometry for a transverse wobbler (TW). The short- $s$ , long- $l$ , and medium- $m$  axes are defined in the body-fixed frame. The vectors  $\vec{R}$ ,  $\vec{j}$ , and  $\vec{I}$  represent the set of angular momenta of the core, odd particle, and the total nuclear system, respectively.

wobbling band was measured initially [9], followed by two additional wobbling bands discovered one year later [10, 11]. Other experimental evidence came quickly after that and now the following nuclei are considered as wobblers:  $^{105}\text{Pd}$  [17],  $^{127}\text{Xe}$  [16],  $^{133}\text{La}$  [13],  $^{135}\text{Pr}$  [14, 15],  $^{161,163,165,167}\text{Lu}$  [2, 4, 5, 10, 11],  $^{167}\text{Ta}$  [3],  $^{183,187}\text{Au}$  [18, 19]. Regarding the wobbling motion for the even-even nuclei the  $^{112}\text{Ru}$  ( $Z = 44$ ) nucleus has three wobbling bands [20], two of them being the excited one- and two-wobbling phonon bands. Another nucleus is  $^{114}\text{Pd}$  [21], with two excited bands of wobbling character, similar to  $^{112}\text{Ru}$ . The even-even nucleus  $^{130}\text{Ba}$  ( $Z = 56$ ) [22–24] was also confirmed very recently to exhibit wobbling behavior.

Compared to the wobbling mode described in [1], which has a purely collective form, in the case of odd- $A$  nuclei, it turns out that the wobbling mode appears due to the coupling of a valence nucleon (the so-called  $\pi(i_{13/2})$  intruder) to a triaxial core, driving the nucleus up to large deformation ( $\epsilon \approx 0.4$ ) [12] and giving rise to excited states of the deformed nuclear system, each belonging to a particular wobbling band.

Frauendorf et al. [25] showed that in the case of odd- $A$  nuclei, depending on the coupling between the triaxial core (with a.m.  $\vec{R}$ ) and the single-particle (“valence” nucleon with a.m.  $\vec{j}$ ), there can be two wobbling regimes: transverse (TW) and longitudinal (LW). The triaxial core is viewed as a Liquid Drop, such that the main rotation is along the intermediate  $m$ -axis (since this one has the largest MOI). When the odd particle aligns its angular momentum along the  $m$ -axis, then the system is said to achieve a *longitudinal wobbling* character (LW). If the odd-particle aligns its a.m. with an axis that is perpendicular to the  $m$ -axis (i.e., either the long  $l$ - or short  $s$ -axis of the triaxial rotor), then the system achieves a so-called *transverse wobbling* character. For a better understanding of the wobbling regimes in terms of angular momentum alignment, Figure 1 depicts three particular cases, namely a simple wobbler - inset A.0 (the case firstly developed by Bohr and Mottelson [1]), a longitudinal wobbler - inset A.1, and a transverse wobbler - inset A.2.

The current work represents the second piece of a two-part series of papers that

focuses on the description of the wobbling properties in odd-mass nuclei. Starting from an existing formalism concerning the interpretation of the wobbling structure of  $^{163}\text{Lu}$  [6, 34], that initial framework (which will be further denoted by  $\mathbb{W}1$ ) is extended with a proper description of the states with positive and negative parity, by adopting the concept of *Parity Partner Bands*. In the newly developed approach (denoted hereafter by  $\mathbb{W}2$ ), a single particle (the odd  $i_{j=13/2}$  proton) couples to the triaxial core, generating a sequence of four triaxial strongly deformed bands (called  $TSD_1, TSD_2, TSD_3$  and  $TSD_4$ ), with a total of 63 rotational states in all the bands. Previously in  $\mathbb{W}1$ , two different particle-core couplings were considered: one that consisted in the  $i_{j=13/2}$  proton+core for the bands  $TSD_{1,2,3}$  and one  $h_{j=9/2}$  proton+core for  $TSD_4$  band, which resulted in two separate fitting procedures required to obtain the energy spectrum of this isotope. Within  $\mathbb{W}2$ , as per the first part of this series of papers (denoted throughout the paper with **I** [7]), a single fitting procedure was required to find the excitation energies of  $^{163}\text{Lu}$ , since only one proton was considered to align its angular momentum with that of the triaxial core. A successful description of the wobbling spectrum of  $^{163}\text{Lu}$  was made in **I**, together with calculation of other relevant quantities (e.g. rotational frequencies) that put  $\mathbb{W}2$  to the test in terms of correctness. The obtained agreement with the experimental data was impressive.

In this second part (hereafter denoted by **II**), attention is given to the properties of the classical energy function of  $^{163}\text{Lu}$ , and the geometrical interpretation of the total angular momentum. The classical expression of the energy function, which can be obtained via the Time-Dependent Variational Principle (TDVE) applied in **I** allows the study of the wobbling stability, and also provides an insight into the classical features of nucleonic motion within the angular momentum space. Its expression signifies the initial quantal Hamiltonian of the deformed system but is brought to a dequantized form with the help of a set of coordinates that describe the dynamics. By expressing the angular momentum vector  $I$  of the triaxial nucleus and the energy function  $E$  as surfaces in a three-dimensional space, it is possible to obtain the trajectories of the rotating system by intersecting the two shapes. This aspect will be analyzed in detail later on.

The structure of this work is as follows. In Section 2 a brief overview of the key characteristics for the  $\mathbb{W}2$  approach that emerged from **I** is made. In Section 3, the prerequisites for obtaining a classical expression of the energy function are formulated. Section 4 is devoted to the numerical results concerning the wobbling stability of  $^{163}\text{Lu}$ . Wobbling stability is studied in terms of contour plots of the aforementioned energy function. The nuclear trajectories (i.e., the intersection curves of the energy surface with angular momentum surface) of the system are graphically represented for given values of angular momentum and energy. Several regimes of rotational motion emerge from this analysis. Discussion of the results is also made in Section 4. The conclusions of this current work are given in Section 5.

## 2. NEW FORMALISM FOR THE DESCRIPTION OF WOBBLING STATES

The  $\mathbb{W}2$  formalism which emerged in **I** [7] consists in a re-interpretation of the four wobbling bands from  $^{163}\text{Lu}$ . Namely, the bands  $TSD_2$  and  $TSD_4$  are *parity partner bands*:  $\Delta I = 2$  sequences with identical spins but opposite parity ( $\pi_2 = +1$  and  $\pi_4 = -1$ ). Arguments for this came from the analysis of the wave function of the system. The function is an admixture of states with both positive and negative parity since the initial Hamiltonian is symmetric to rotations by a specific amount ( $D_2$  implies invariance to rotations by  $\pi$ ). A complete description of the properties of the wave function and the Hamiltonian concerning the parity property is made in **I**. In terms of wobbling excitations, both  $TSD_2$  and  $TSD_4$  are considered to be ground-state bands (zero-wobbling-phonon), obtained by coupling the  $j_1 = 13/2$  proton (with parity  $\pi_{j_1} = +1$ ) to a triaxial core of odd spins  $R_2^+ = 1^+, 3^+, 5^+, \dots$  for  $TSD_2$  and  $R_2^- = 1^-, 3^-, 5^-, \dots$  for  $TSD_4$ . The band  $TSD_1$  is also regarded as a ground state band, but here the proton couples to a core of even spin states  $R_1 = 0^+, 2^+, 4^+, \dots$ , and  $TSD_3$  is indeed an excited wobbling band (one-wobbling-phonon) that is built on top of  $TSD_2$  via the action of a phonon operator. The coupling schemes for  $\mathbb{W}2$  are described in **I** (denoted by  $C'_1$ ,  $C'_2$ , and  $C'_3$ ). For a clearer picture, Appendix A contains a diagram with all three mechanisms (see Fig. 11).

It is worth noting that this interpretation of the wobbling structure of  $^{163}\text{Lu}$  contrasts the previously known band configuration [25, 27, 35] where the bands  $TSD_2$  and  $TSD_3$  were regarded as one- and two-wobbling phonon excitations built on the yrast  $TSD_1$  band. However, it was recently shown [6, 30, 34] that  $TSD_1$  and  $TSD_2$  behave as signature partner bands, both being ground states with the favored (unfavored)  $\alpha_f = +\frac{1}{2}$  ( $\alpha_u = -\frac{1}{2}$ ) band as  $TSD_1$  ( $TSD_2$ ). This aspect, together with the fact that  $TSD_2$  and  $TSD_4$  are parity partners comprise the main ideas behind the  $\mathbb{W}2$  formalism adopted in **I** and **II**. The workflow involved in  $\mathbb{W}2$  is drawn in Fig. 10, and for the sake of completeness, the initial  $\mathbb{W}1$  approach is also sketched in Fig. 9 from Appendix A.

## 3. THEORETICAL FORMALISM

Concerning the odd nucleus  $^{163}\text{Lu}$ , system can be treated within the Particle Rotor Model (PRM) [8, 25, 26]. This approach is an extension of the Triaxial Rotor Model (TRM) that was firstly developed by Bohr and Mottelson [1], and then treated in a fully quantal approach by Davydov and Filippov [28]. Thus, the deformed system is described with a similar Hamiltonian used in  $\mathbb{W}1$ , namely the Hamiltonian for

the triaxial PRM:

$$H = H_{\text{core}} + H_{\text{s.p.}} = \sum_{i=1,2,3} \frac{1}{2\mathcal{I}_i} (I_i - j_i)^2 + \frac{V}{j(j+1)} \left[ \cos \gamma (3j_3^2 - \vec{j}^2) - \sqrt{3} \sin \gamma (j_1^2 - j_2^2) \right] + \epsilon_j . \quad (1)$$

The Hamiltonian from Eq. 1 describes a system in which an odd particle with a.m.  $\vec{j}$  interacts with a triaxial even-even core of a.m.  $\vec{R}$ , that is the odd nucleon is moving in a quadrupole deformed mean-field which is generated by the core. As such, the first term in the Hamiltonian  $H_{\text{core}}$  describes the motion of a triaxial core, while the second term  $H_{\text{s.p.}}$  represents the single-particle potential characterizing the valence proton (the well-known deformed Nilsson potential [36, 37]).  $\epsilon_j$  represents the single-particle energy of the nucleon itself, a value that depends on the orbital where it belongs to. In Eq. 1 the core angular momentum is  $\vec{R} = \vec{I} - \vec{j}$  and the terms  $\mathcal{I}_i$  represent the moments of inertia for a triaxial ellipsoid, along the principal axes.  $\gamma$  is the triaxiality parameter [1] which can be considered as a measure of asymmetry between the three moments of inertia. The strength parameter  $V$  from the expression of the deformed potential is related to the quadrupole deformation parameter  $\beta_2$  [1].

Solving the problem of W2 is equivalent to finding the eigenvalues of  $H$  given in Eq. 1. In a similar approach as in W1, the eigenvalues of interest are obtained on the base of a semi-classical approach. This is preferred since it working within a semi-classical approach allows one to keep close contact with the system's dynamics in terms of equations of motion for the generalized coordinates. However, exact calculations of the initial quantal Hamiltonian were performed for W1 and the agreement with the experimental data was checked (see Refs. [6, 30]). Thus, the first step is to perform a de-quantization procedure of  $H$  through the TDVE [29, 31, 33]:

$$\delta \int_0^t \langle \Psi_{IjM} | H - i \frac{\partial}{\partial t'} | \Psi_{IjM} \rangle dt' = 0 . \quad (2)$$

The trial function from Eq. 2 is carefully chosen as a product of two basis states comprising the states with total angular momentum  $I$  and  $j$ , respectively:

$$|\Psi_{IjM}\rangle = \mathbf{N} e^{z\hat{I}_-} e^{s\hat{j}_-} |IMI\rangle |jj\rangle , \quad (3)$$

where the operators  $\hat{I}_-$  and  $\hat{j}_-$  denote the lowering operators for the intrinsic angular momenta  $\vec{I}$  and  $\vec{j}$ , respectively, and  $\mathbf{N}$  plays the role of the normalization constant. One must remark the fact that the states  $|IMI\rangle$  and  $|jj\rangle$  from Eq. 3 are extremal states for the operators  $(\hat{I}^2, \hat{I}_3)$  and  $(\hat{j}^2, \hat{j}_3)$ , respectively, and they correspond to the maximally allowed states for a given set of angular momenta  $I$  and  $j$ . As an observation, the trial function is an admixture of components of definite  $K$ , which is consistent with the fact that for a triaxial nucleus,  $K$  is not a good quantum number.

The variables  $z$  and  $s$  from Eq. 3 are complex functions of time, and they play the role of classical coordinates in the phase space that describe the motion of the core and the odd particle, respectively:

$$z = \rho e^{i\varphi}, \quad s = f e^{i\psi}. \quad (4)$$

In order to obtain a set of classical equations in a Hamilton Canonical form, a new pair of variables are introduced:

$$r = \frac{2I}{1 + \rho^2}, \quad t = \frac{2j}{1 + f^2}, \quad (5)$$

where  $r \in [0, 2I]$  and  $t \in [0, 2j]$ . Thus the equations of motion acquire the form:

$$\begin{aligned} \frac{\partial \mathcal{H}}{\partial r} &= \dot{\varphi}; \quad \frac{\partial \mathcal{H}}{\partial \varphi} = -\dot{r}, \\ \frac{\partial \mathcal{H}}{\partial t} &= \dot{\psi}; \quad \frac{\partial \mathcal{H}}{\partial \psi} = -\dot{t}. \end{aligned} \quad (6)$$

The explicit form of the above equations of motion are given in Appendix A of [32]. The function  $\mathcal{H}$  denotes the average of the Hamiltonian operator  $H$  (Eq. 1) with the trial function  $|\Psi_{IjM}\rangle$  given in Eq. 3, and it plays the role of classical energy function:

$$\mathcal{H}(\varphi, r; \psi, t) = \langle \Psi_{IjM} | H | \Psi_{IjM} \rangle, \quad (7)$$

$\mathcal{H}$  is a constant of motion, meaning that  $\dot{\mathcal{H}} \equiv 0$ . This equation will define a surface, a so-called *equi-energy surface*  $\mathcal{H} = \text{const}$ . It is worth mentioning the fact that such equality holds because the entire set of equations of motion emerged from a variational principle. The sign of the Hessian associated with this classical function will indicate its stationary points. Among them some are minima, and the critical points which are of interest for the present study are minimal, and obtained when the following ordering for the three moments of inertia holds:  $\mathcal{I}_1 > \mathcal{I}_2 > \mathcal{I}_3$ . There are no restrictions for the triaxiality parameter  $\gamma$  and the single-particle potential strength  $V$  (which can implicitly be considered as a measure of the quadrupole deformation parameter  $\beta_2$ ). As such, the set of coordinates  $(\varphi, r; \psi, t)$  will provide a minimum value for  $\mathcal{H}$  only for certain values that will be discussed in the following part. Regarding the physical meaning of  $(\varphi, r; \psi, t)$ , one can see that the angles  $\varphi$  and  $\psi$  play the role of generalized coordinates, while  $r$  and  $t$  represent the conjugate momenta.

### 3.1. ENERGY FUNCTION - GEOMETRICAL INTERPRETATION

The analytical expression for the average of  $H$  with the trial function describing the system was previously calculated in W1. Indeed, the energy function  $\mathcal{H}$  was given

in terms of the phase space coordinates  $(r, \varphi; t, \psi)$  as follows [34]:

$$\begin{aligned} \mathcal{H} = & \frac{I}{2}(A_1 + A_2) + A_3 I^2 + \frac{2I-1}{2I} r(2I-r) \mathcal{A}_\varphi + \frac{j}{2}(A_1 + A_2) + A_3 j^2 + \\ & + \frac{2j-1}{2j} t(2j-t) \mathcal{A}_\psi - 2\sqrt{r(2I-r)t(2j-t)} \mathcal{A}_{\varphi\psi} + \\ & + A_3 [r(2j-t) + t(2I-r)] - 2A_3 Ij + V \frac{2j-1}{j+1} \mathcal{A}_\gamma \end{aligned} \quad (8)$$

with:

$$\begin{aligned} \mathcal{A}_\varphi(\varphi) &= (A_1 \cos^2 \varphi + A_2 \sin^2 \varphi - A_3) , \\ \mathcal{A}_{\varphi\psi}(\varphi, \psi) &= (A_1 \cos \varphi \cos \psi + A_2 \sin \varphi \sin \psi) , \\ \mathcal{A}_\psi(\psi) &= (A_1 \cos^2 \psi + A_2 \sin^2 \psi - A_3) , \\ \mathcal{A}_\gamma(t, \psi) &= \left[ \cos \gamma - \frac{t(2j-t)}{2j^2} \sqrt{3} (\sqrt{3} \cos \gamma + \sin \gamma \cos 2\psi) \right] . \end{aligned} \quad (9)$$

For the condition  $A_1 > A_2 > A_3$ , the expression from Eq. 8 is minimal in the point  $p_0|_{\min} = (0, I; 0, j)$ , since  $p_0$  is a critical point of  $\mathcal{H}$ . The same critical point was used within **I** in order to obtain the expression of  $\mathcal{H}_{\min}^{(I,j)}$  which entered in the expressions of the excitation energies for  $^{163}\text{Lu}$  (See Eqs. 7-9 from **I**). Therein, it was possible to parametrize the total energy of the system in terms of the three MOIs, the triaxiality parameter  $\gamma$ , and the single-particle potential strength  $V$ , having them as free parameters (denoted as  $\mathcal{P}$  in **I**). Performing a least square fitting procedure for the entire energy spectrum of  $^{163}\text{Lu}$ , a set  $\mathcal{P}$  was obtained which provided the best overall agreement with experimental data concerning these excitation energies. In fact, looking back at Eqs. 8 and 9 written above, the same parameters are also present here. Since the inertial parameters  $A_k$  are  $A_k = \frac{1}{2I_k}$ ,  $k = 1, 2, 3$ , it follows that:

$$\mathcal{H} = \text{fct}(\mathcal{I}_1, \mathcal{I}_3, \mathcal{I}_3, \gamma, V) . \quad (10)$$

161 This will help in the numerical application of the current research since one  
162 can just adopt the numerical values for  $\mathcal{P} \equiv [\mathcal{I}_{1,2,3}, \gamma, V]$  obtained via the fitting pro-  
163 cedure that was applied for the excitation energies in **I**. Indeed, the classical energy  
164 function plays a crucial role in both determining the wobbling energies of the iso-  
165 tope, but also (as it will be shown) studying its behavior concerning the geometry of  
166 the system.

Furthermore, it is instructive to check the dependence of the energy function on the angular momentum components, e.g., the coordinates  $x_k \stackrel{\text{not.}}{=} I_k$ ,  $k = 1, 2, 3$ , where the quantization axis is chosen as the 3-axis. By expressing the angular momentum coordinates  $x_{1,2,3}$  in terms of the polar angles  $(\theta, \varphi)$  and a radius  $I$ , one

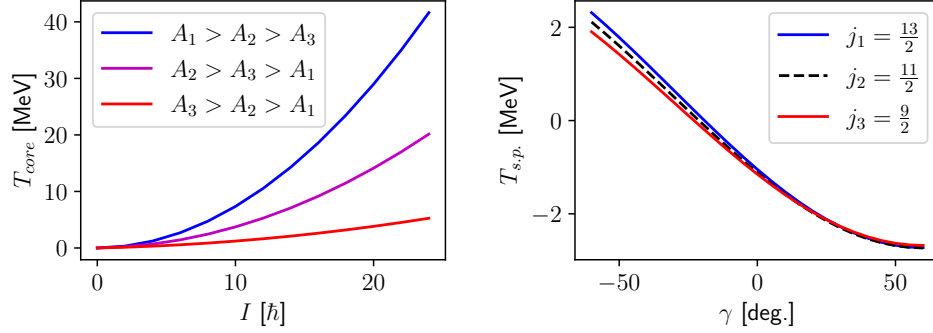


Fig. 2 – **Left:** The free term from Eq. 13 which corresponds to the core, for different orderings of the MOIs. For the ordering  $A_1 > A_2 > A_3$ , the parameters from Table 1 were taken. **Right:** The free term from Eq. 14 which corresponds to the single-particle. The evaluation of  $T_{\text{s.p.}}$  was made for the parameters listed in Table 1.

obtains:

$$x_1 = I \sin \theta \cos \varphi, \quad x_2 = I \sin \theta \sin \varphi, \quad x_3 = I \cos \theta. \quad (11)$$

Using this coordinates system and evaluating the energy function around its minimum point  $p_0 = (0, I; 0, j)$ , the following expression for  $\mathcal{H}$  will be obtained:

$$\mathcal{H} |_{p_0} = I \left( I - \frac{1}{2} \right) \sin^2 \theta \cdot \mathcal{A}_\varphi(\varphi) - 2A_1 I j \sin \theta + T_{\text{core}} + T_{\text{s.p.}}. \quad (12)$$

The last two terms in this equation are independent on the polar angles  $(\theta, \varphi)$  and they have the following form:

$$T_{\text{core}} = \frac{I}{2} (A_1 + A_2) + A_3 I^2, \quad (13)$$

$$T_{\text{s.p.}} = \frac{j}{2} (A_2 + A_3) + A_1 j^2 - V \frac{2j-1}{j+1} \sin \left( \gamma + \frac{\pi}{6} \right). \quad (14)$$

167 A quantitative analysis on these two quantities is useful in order to see how a  
 168 different  $A_k$  ordering would affect  $T_{\text{core}}$ , and also how is the single-particle angular  
 169 momentum influencing  $T_{\text{s.p.}}$ . Results for both quantities are graphically represented  
 170 in Fig. 2.

171 The classical equations of motion admit two constants of motion: the total en-  
 172 ergy ( $E$ ) and the total angular momentum ( $I$ ). Consequently, by finding the intersec-  
 173 tion line(s) between the energy surface  $E$  and the surface of the angular momentum,  
 174 the system's trajectory at that particular energy and spin is obtained. Such represen-  
 175 tations will be made in the following section.

By changing the form of Eq. 12 from polar coordinates into Cartesian coordi-



nates, the energy surface  $E$  will become:

$$E = \left(1 - \frac{1}{2I}\right) A_1 x_1^2 + \left(1 - \frac{1}{2I}\right) A_2 x_2^2 + \left[\left(1 - \frac{1}{2I}\right) A_3 + A_1 \frac{j}{I}\right] x_3^2 - I \left(I - \frac{1}{2}\right) A_3 - 2A_1 I j + T_{\text{rot}} + T_{\text{sp}}. \quad (15)$$

Indeed, one can notice that the three coordinates  $x_k$  appear as a squared sum. If some notations are made for the terms appearing next to the coordinates and the coordinate-free terms, one arrives at the following expression for the energy surface:

$$E = \mathcal{S}_1 x_1^2 + \mathcal{S}_2 x_2^2 + \mathcal{S}_3 x_3^2 + \mathcal{S}_0^{\text{rot+sp}}. \quad (16)$$

From Eq. 16, it is now clear that the energy surface will be an ellipsoid with the *semi-axes* of lengths  $1/\mathcal{S}_{1,2,3}$ , while the free-term  $\mathcal{S}_0^{\text{rot+sp}}$  will produce an overall shift of the entire surface. The shift is caused by the core+particle coupling, and its magnitude is strictly dependent on the parameter set  $\mathcal{P}$ . It is remarkable the fact that the quality of the fitting results from **I** is reflected in the present work through the classical geometric interpretation of the triaxial particle-core ellipsoid, via the parameters  $\mathcal{P}$ .

Furthermore, for a total angular momentum  $\vec{I}$ , the vector generates a sphere of radius  $r = I$  described by the equation:

$$I^2 = x_1^2 + x_2^2 + x_3^2. \quad (17)$$

The trajectories obtained through the intersection of Eqs. 16 (the shifted ellipsoid  $E$ ) and 17 (i.e., a sphere of radius  $r = I$ ) will give a classical visualization of the wobbling character for a triaxial nucleus, and the possible trajectories of the system concerning its motion inside the angular momentum space.

#### 4. NUMERICAL RESULTS

As already mentioned in the previous section, for the numerical part of this research, the parameters obtained from the fitting procedure made in **I** will be adopted for consistency of the  $\mathbb{W}2$  approach, their values being listed in Table 1. It is worth noting that for the case of  $\mathbb{W}1$ , the geometrical interpretation of the classical energy function would have required two such sets of parameters, and therefore, two sets of calculations (one for the bands  $TSD_{1,2,3}$  and one for  $TSD_4$ ).

Here, by using the parameters from Table 1, numerical calculations of  $\mathcal{H}$  expressed in the polar coordinates via Eq. 12 are performed, with graphical visualization of its behavior. Furthermore, the surfaces  $E$  and  $I^2$  described in Eqs. 15-17 will be represented for different values of the energy and the total spin.

Table 1

The parameter set  $\mathcal{P}$  that was determined by a fitting procedure of the excitation energies for  $^{163}\text{Lu}$ , provided via calculations from I.

$\mathcal{I}_1 [\hbar^2/\text{MeV}]$	$\mathcal{I}_2 [\hbar^2/\text{MeV}]$	$\mathcal{I}_3 [\hbar^2/\text{MeV}]$	$\gamma [\text{deg.}]$	$V [\text{MeV}]$
72	15	7	22	2.1

#### 4.1. STABILITY OF THE WOBBLING REGION

The expression for the classical energy function, which plays a crucial role in analyzing the nucleus's stability for a given rotational state, was presented in the previous section, through Eq. 12. This will be used within the present numerical calculations to pinpoint the regions in space where the minimal points of  $\mathcal{H}$  do exist. A special interest is devoted to the low-lying states from each of the four bands. Namely, for each band, a spin-state close to the band-head is chosen, then using the parameter set  $\mathcal{P}$ , a graphical representation in the  $(\theta, \varphi)$ -coordinate space is realized, and in each case, the extremal points with minimum character are identified. These graphical representations are shown in Figs. 3 and 4. For the sake of completeness, the critical points of  $\mathcal{H}$  which are minimal are listed separately in Table 2.

Table 2

The minimum points of  $\mathcal{H}$ , numerically evaluated for the parameter set  $\mathcal{P}$ . The points are represented as the *red dots* on the contour plots from Figs. 3-4.

Minimal point	$\theta [\text{rad}]$	$\varphi [\text{rad}]$	$A_k$ ordering
$p_0$	$\pi/2$	0	$A_3 > A_2 > A_1$
$p_1$	$\pi/2$	$\pi$	$A_3 > A_2 > A_1$
$p_2$	$\pi/2$	$2\pi$	$A_3 > A_2 > A_1$

The four contour plots shown in Figs. 3 and 4 have many similarities, suggesting common collective properties, but also differences which are caused by the fact that the minima have different depths. A common feature consists in that the equi-energy curves surround a sole minimum for low values in energy, but as the energy increases, the trajectories go around all minima, the lack of localization indicating unstable wobbling motion. The unstable regions might also relate to phase transitions, where the nucleus can undergo a major change in its rotational character. This aspect will also be discussed in the next subsection, devoted to the 3-dimensional representation of the energy ellipsoid and the classical trajectories of the triaxial system.

Regarding the minimum points of  $\mathcal{H}$  from Table 2, their position remains unchanged for all four bands and any rotational state  $I$ , as long as the ratio of the inertial

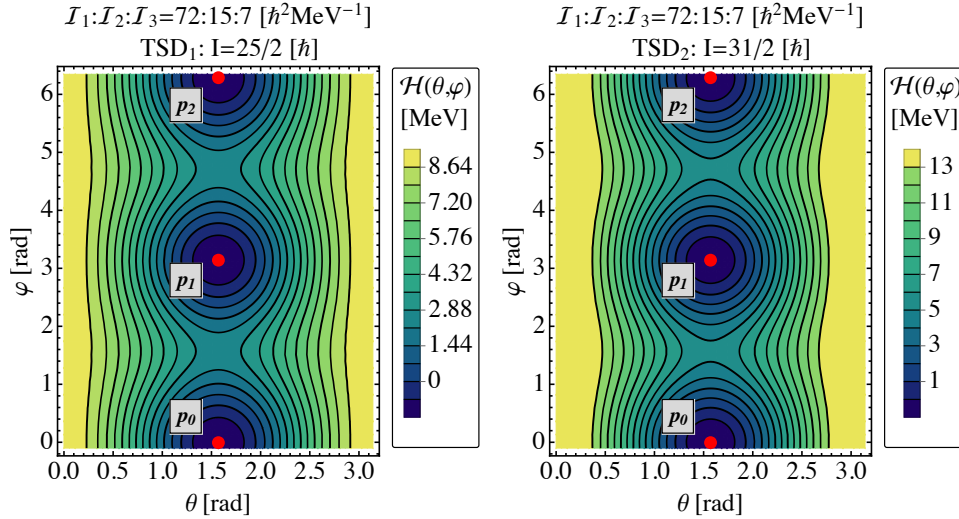


Fig. 3 – The classical energy function  $\mathcal{H}$  given by Eq. 12 for a state in  $TSD_1$  (left) and a state from  $TSD_2$  (right). Calculations were performed with the numerical parameters given in Table 1. The minimum points for  $\mathcal{H}$  are marked by red dots (see also Table 2), and they represent the regions in space where the nucleus has the most stable wobbling character (i.e., the precessional motion of the total a.m. is relatively small). The closed contours represent trajectories surrounding the minimum points, where wobbling motion can occur, while the contours surrounding all three minima represent the unstable motion of the nucleus, where the wobbling regime is forbidden.

parameters  $A_k$  (or implicitly the MOIs) stays the same. Remarkable is the fact that only with the adopted set of parameters  $\mathcal{P}$  (i.e., the MOI order  $\mathcal{I}_1 > \mathcal{I}_2 > \mathcal{I}_3$ ) it was possible to define regions with stable motion (marked by the dark-colored regions from Figs. 3 and 4). Indeed, if the two ratios  $\mathcal{I}_1/\mathcal{I}_2$  and  $\mathcal{I}_2/\mathcal{I}_3$  would have been smaller, a larger unstable region would prevail (with regions of maximal character), constraining thus the stable wobbling motion. This could indicate the fact that the single-particle term  $T_{s,p}$  from the expression of  $\mathcal{H}$  is sensitive to larger triaxiality, and only for certain values will the system achieve a stable motion characterized by large deformation (see Eq. 14). In fact, Fig. 2 shows the change in magnitude of  $T_{s,p}$  concerning the triaxiality parameter  $\gamma$ .

An additional step consists in the analysis of the energy function, more precisely to see its evolution in one of the minimum points with respect to the angular momentum  $I$ . As it was already observed from the contour plots shown in Figs. 3-4, the depth of the minima differs from one spin state to another, so it would be useful to have a quantitative view on that change. By fixing  $\mathcal{H}$  in one of its critical points (e.g., the minimum point  $p_0 = (\frac{\pi}{2}, 0)$ ), the angular momentum  $I$  was varied within a large interval, and the evolution of  $\mathcal{H}$  was evaluated. Graphical representation is shown in Figure 5.

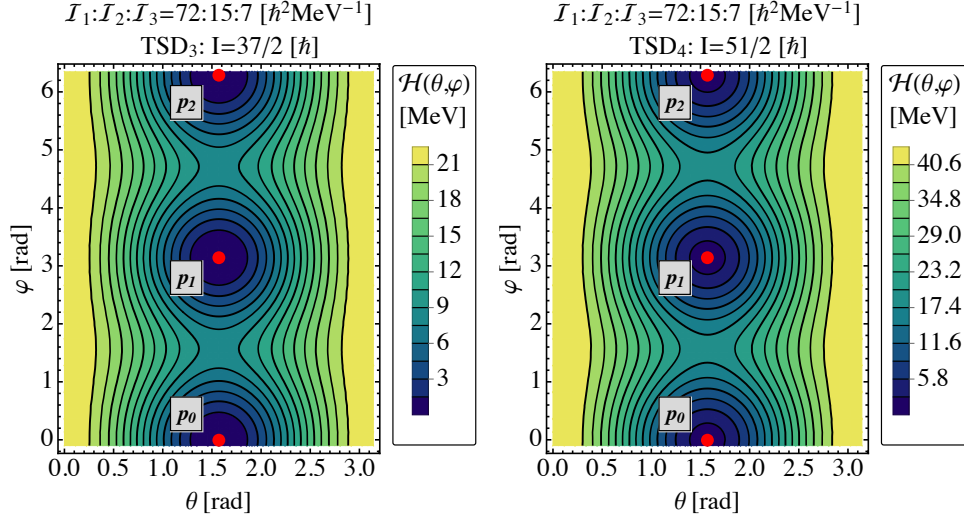


Fig. 4 – The classical energy function  $\mathcal{H}$  given by Eq. 12 for a state in  $TSD_3$  (left) and a state from  $TSD_4$  (right). Calculations were performed with the numerical parameters given in Table 1. The minimum points for  $\mathcal{H}$  are marked by red dots (see also Table 2), and they represent the regions in space where the nucleus has the most stable wobbling character (i.e., the precessional motion of the total a.m. is relatively small). The closed contours represent trajectories surrounding the minimum points, where wobbling motion can occur, while the contours surrounding all three minima represent the unstable motion of the nucleus, where the wobbling regime is forbidden.

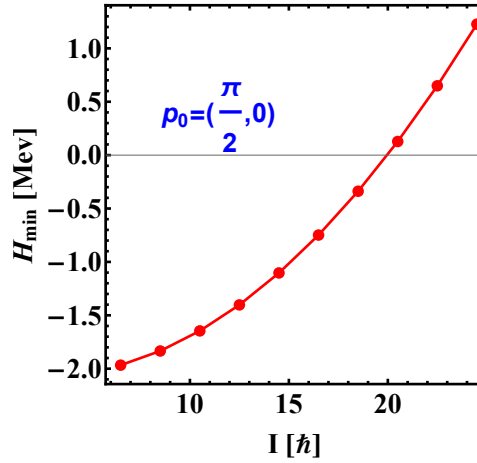


Fig. 5 – The change in the minimum depth of  $\mathcal{H}$ , evaluated in the one of its critical points  $p_0(\theta, \varphi) = (\frac{\pi}{2}, 0)$ , using the parameters given in Table 1.

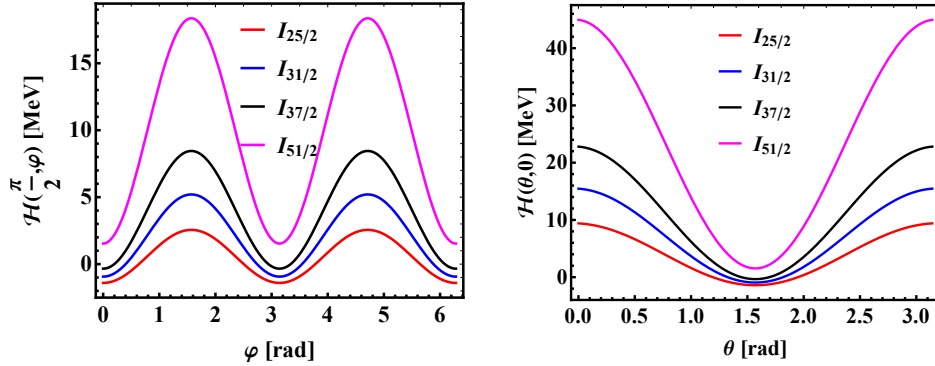


Fig. 6 – The energy function  $\mathcal{H}$ , evaluated in one of its minimum points, with respect to only one of the polar coordinates. One coordinate is fixed while the other one is varied within its interval of existence ( $\theta \in [0, \pi]$  and  $\varphi \in [0, 2\pi]$ ). The chosen minimum is  $p_0 = (\frac{\pi}{2}, 0)$ . Each spin state corresponds to one of the four triaxial bands of  $^{163}\text{Lu}$  (with  $I_{25/2} \in TSD_1$ ,  $I_{31/2} \in TSD_2$ ,  $I_{37/2} \in TSD_3$ , and  $I_{51/2} \in TSD_4$ ).

As it can be seen from Figure 5, the classical energy  $\mathcal{H}$  is an increasing function of angular momentum, which is to be expected, since the wobbling energies of the four bands increase with respect to the increase in spin. The negative values of  $\mathcal{H}$  for low-lying states do not indicate that the nucleus has negative energy since the rest of the nucleus' energy is also given by the single-particle energy  $\epsilon_j$  that appears in the initial Hamiltonian and the phononic terms (see Eq. 8 from I for the physical meaning of the phononic terms  $\mathcal{F}$ ).

Another useful insight would be the study of the classical energy function  $\mathcal{H}$  as separate functions of the polar coordinates  $\theta$  and  $\varphi$ , respectively. This can be achieved by choosing a minimum point, keeping one of the polar coordinates fixed, and then let the other one vary across its corresponding interval. For  $^{163}\text{Lu}$ , such a graphical representation was done for the point  $p_0 = (\frac{\pi}{2}, 0)$  (that is the bottom-most red dot from each of the four contour plots depicted in Figs. 3-4). Results can be seen in Figure 6.

#### 4.2. CLASSICAL TRAJECTORIES - 3D REPRESENTATION

The final step of the present work is to obtain an insight into the classical features of  $^{163}\text{Lu}$  concerning the total angular momentum and its rotational motion. As already mentioned, the trajectories are given by the intersection curves of the energy ellipsoid  $E$  given in Eq. 15 with the angular momentum sphere  $I$  given in Eq. 17. In the 3-dimensional space generated by the three components of the angular momentum vector  $\vec{I}$ , these intersection curves characterize the motion of the system, as each curve will be oriented along with one of the three axes  $x_k$ ,  $k = 1, 2, 3$ , suggesting a rotational motion (the precession of the total a.m.) around a particular direction

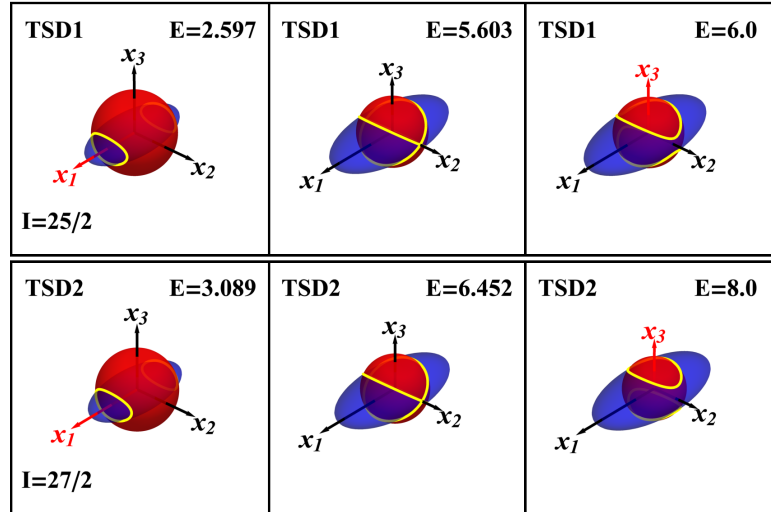


Fig. 7 – The nuclear trajectories of the system, evaluated for two spin states belonging to  $TSD_1$  and  $TSD_2$ . Intersection lines marked by yellow color represents the actual orbits. Axis colored in red represents the direction along which the system rotates (it precesses). The left-most inset corresponds to the real excitation energy for that particular spin state  $I$ .

preferred by the system.

The meaning of a trajectory can be described from a geometrical standpoint as the *collection* of points in space along which the total angular momentum  $\vec{I}$  orbits, making a precessional motion (Fig. 1 shows the orbiting character of  $\vec{I}$ ). As discussed in the introductory part of this paper, the precession is caused by the asymmetry in the three MOIs of the triaxial nucleus this causing the nucleus to wobble with a harmonic-like frequency (the wobbling frequencies for  $^{163}\text{Lu}$  were analyzed in **I**).

The dependence of the classical trajectories on the angular momenta as well as on energies must be analyzed in **W2**. Indeed, when the model Hamiltonian is diagonalized for a given  $I$ , a set of  $2I + 1$  energies are obtained. Therefore, it is justified to study the evolution of trajectories when the energy of the nucleus is increasing. The curves are represented as the manifold given by the intersection of the two constants of motion  $E$  and  $I$ . Examples of such trajectories are depicted in Figs. 7-8.

Each row from the Figs. 7-8 represents a rotational state within a band. A low-lying spin state was chosen from each band in particular as an example. The left inset of each row represents the real excitation energy for the state  $I$  at which the energy ellipsoid is evaluated. It can be seen that two distinct (but symmetric) trajectories are observed along the  $x_1$ -axis, for all four states. This suggests that the states of the triaxial nucleus are obtained from the rotation of the angular momentum along

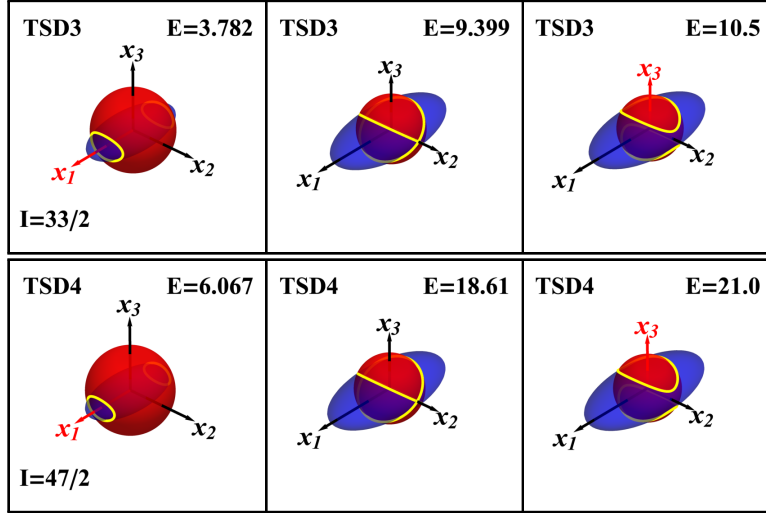


Fig. 8 – The nuclear trajectories of the system, evaluated for two spin states belonging to  $TSD_3$  and  $TSD_4$ . Intersection lines marked by yellow color represents the actual orbits. Axis colored in red represents the direction along which the system rotates (it precesses). The left-most inset corresponds to the real excitation energy for that particular spin state  $I$ .

279  $x_1$ . Indeed, for low energies, the rotation is more pronounced along the  $x_1$ - and  $-x_1$ -  
 280 axes. As the energy of the nucleus increases, the two trajectories approach each other,  
 281 which results in a tilted rotation axis corresponding to both curves. The tilted axis  
 282 implies that the rotation axis is being misaligned, the rotational axis moving away  
 283 from its *equilibrium point*, marking the tilted-axis rotation. Note that this picture is  
 284 fully consistent with the one described by Lawrie et al. [38]. Further increase in  
 285 energy will result in the two trajectories intersect with each other. The point where  
 286 the intersection between the two orbits occurs is marked in the middle inset from  
 287 each figure. Consequently, the intersection of these two orbits marks an unstable  
 288 motion within the system. Finally, when the energy increases even more, beyond  
 289 this *critical point*, one arrives again in a two-trajectories regime but with a different  
 290 rotation axis, lying closer to the  $x_3$  axis. This case is shown in the right inset within  
 291 each figure, where the axis  $x_3$  is marked by red color, signaling the change in the  
 292 rotational mode of the nucleus. However, it is worth noting that such energies are  
 293 way too large for such a phase transition to occur naturally in  $^{163}\text{Lu}$ . For example,  
 294 in the case of  $I_{25/2} \in TSD_1$ , the energy at which  $^{163}\text{Lu}$  undergoes a phase transition  
 295 with regards to the rotational mode is close to 5.6 MeV (middle inset for  $TSD_1$   
 296 from Figure 3), but the real excitation energy which corresponds to this state is half  
 297 that value (left inset for  $TSD_1$  from Figure 7). Nevertheless, it is a remarkable fact  
 298 that with the current model, a phase transition between rotational modes in a triaxial

nucleus can be identified. A proper microscopic formalism based on this approach might also provide a more detailed picture with regards to the allowed trajectories for the system.

It is worth mentioning that in **I**, the analysis of the wobbling energy of  $^{163}\text{Lu}$  as defined in [25] pointed out that there might be a *critical spin* value  $I_{\text{cr}}$  where the energy changes its behavior: going from an increasing function of  $I$  to a decreasing function of  $I$  (for reference, see Fig. 4 from **I**). Therein, based on the obtained values of the moments of inertia, it was concluded that this critical spin value marks the point where the system undergoes a change in its wobbling regime from Longitudinal Wobbling to Transverse Wobbling. Here, the critical energy obtained from Figs. 7 and 8 might also indicate a change in the wobbling regime from LW to TW (since the MOIs used for calculations are the same). However, one must obtain the classical trajectories for each spin-state of the wobbling bands in  $^{163}\text{Lu}$ , then find the critical energy at which unstable wobbling occurs, and finally, conclude the actual changes. Such a tedious process might be considered as a motivation for future work.

## 5. CONCLUSIONS & OUTLOOK

Concluding the present work, this newly developed formalism proves to be a successful tool for accurately describing the wobbling spectrum of  $^{163}\text{Lu}$  and also for providing an insight into the rotational motion of the nuclear system with respect to its total spin.

*Acknowledgments.* This work was supported by UEFISCU, through the project **PCE-16/2021**.

## A. APPENDIX - WORKFLOW DIAGRAMS

The two models described throughout the paper, namely the formalisms W1 and W2 are schematically represented. The W1 model corresponds to the work given in Refs. [6, 34], and the W2 corresponds to the formalism developed in this two-part series of papers. For W1, the diagram is shown in Figure 9, while for the newly developed approach W2, the diagram is shown in Figure 10. The coupling scheme for W2 is also represented in Figure 11.

## REFERENCES

1. Aage Niels Bohr and Ben R Mottelson. *Nuclear Structure (In 2 Volumes)*.
2. P Bringel, GB Hagemann, H Hübel, A Al-Khatib, P Bednarczyk, A Bürger, D Curien, G Gangopadhyay, B Herskind, DR Jensen, et al. *The European Physical Journal A-Hadrons and Nuclei*, 24(2):167–172, 2005.



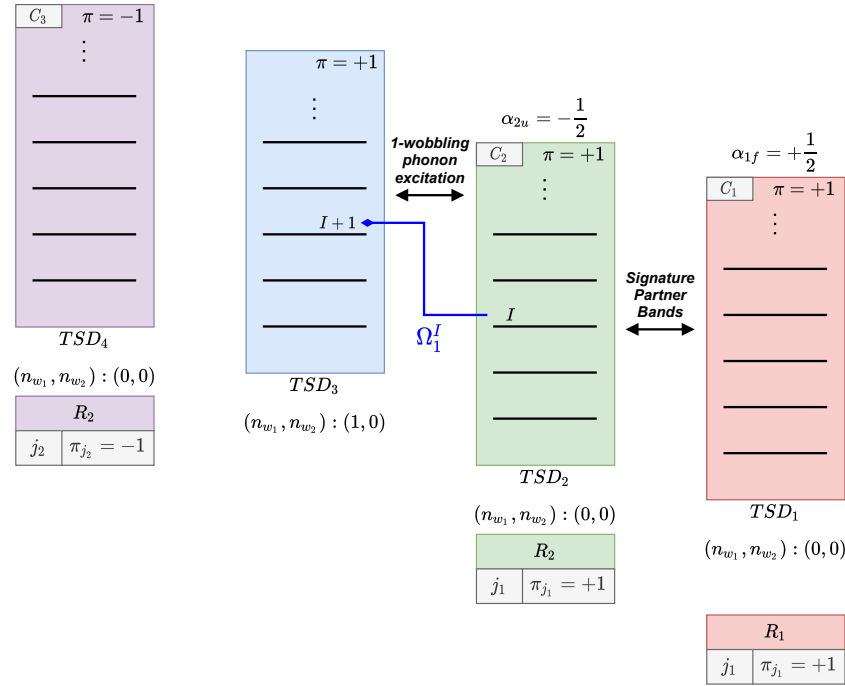


Fig. 9 – Schematic representation of the band structure adopted for  $^{163}\text{Lu}$  in the  $w_1$  model [6, 34]. For each band, the wobbling phonon numbers are shown. The main features and linking properties between bands are represented with arrows. The bottom part shows the coupling scheme (the core and the valence nucleon) for each wobbling band. The blue arrow marks the activation of  $TSD_3$  states via the phonon operator.

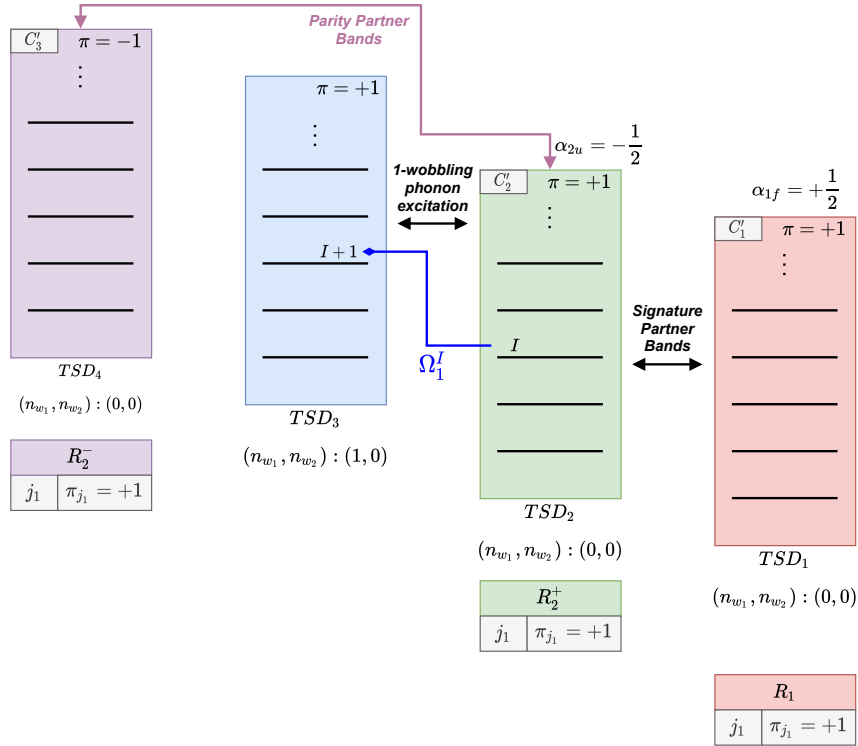


Fig. 10 – Schematic representation of the band structure adopted for  $^{163}\text{Lu}$  in the  $w_2$  model [7]. For each band, the wobbling phonon numbers are shown. The main features and linking properties between bands are represented with arrows. The bottom part shows the coupling scheme (the core and the valence nucleon) for each wobbling band. The blue arrow marks the activation of  $TSD_3$  states via the phonon operator.

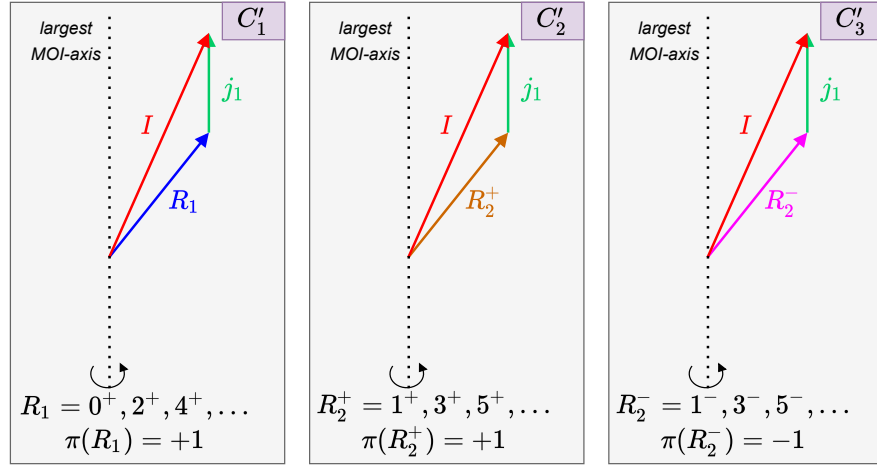


Fig. 11 – A schematic representation with the three coupling schemes that characterize the  $W_2$  model [7]. The same odd particle ( $j_1 = i_{13/2}$  proton) is coupled with two positive cores with even (odd) integer spin sequences for  $TSD_1$  ( $TSD_2$ ), and one negative core in the case of  $TSD_4$  with odd integer spin sequence. The total spin of the system precesses around the axis with the largest MOI, as it is the case for a triaxial rotor. The naming  $C'_{1,2,3}$  of the three cases depicted here is defined and explained in I.

- 329 3. DJ Hartley, RVF Janssens, LL Riedinger, MA Riley, A Aguilar, MP Carpenter, CJ Chiara,  
330 P Chowdhury, IG Darby, U Garg, et al. *Physical Review C*, 80(4):041304, 2009.
- 331 4. H Amro, WC Ma, GB Hagemann, RM Diamond, J Domscheit, P Fallon, A Görgen, B Herskind,  
332 H Hübel, DR Jensen, et al. *Physics Letters B*, 553(3-4):197–203, 2003.
- 333 5. G Schönwaßer, H Hübel, GB Hagemann, P Bednarczyk, G Benzoni, A Bracco, P Bringel, R Chap-  
334 man, D Curien, J Domscheit, et al. *Physics Letters B*, 552(1-2):9–16, 2003.
- 335 6. AA Raduta, R Poenaru, and CM Raduta. *Journal of Physics G: Nuclear and Particle Physics*,  
336 47(2):025101, 2020.
- 337 7. R Poenaru and AA Raduta, *Romanian Journal of Physics*, Paper submitted, 2021.
- 338 8. Gudrun B Hagemann and Ikuko Hamamoto. *Nuclear Physics News*, 13(3):20–24, 2003.
- 339 9. SW Ødegård, GB Hagemann, DR Jensen, M Bergström, B Herskind, G Sletten, S Törmänen,  
340 JN Wilson, PO Tjøm, I Hamamoto, et al. *Physical review letters*, 86(26):5866, 2001.
- 341 10. DR Jensen, GB Hagemann, I Hamamoto, SW Ødegård, B Herskind, G Sletten, JN Wilson,  
342 K Spohr, H Hübel, P Bringel, et al. *Physical review letters*, 89(14):142503, 2002.
- 343 11. D Ringkøbing Jensen, GB Hagemann, I Hamamoto, SW Ødegård, M Bergström, B Herskind,  
344 G Sletten, S Törmänen, JN Wilson, PO Tjøm, et al. *Nuclear Physics A*, 703(1-2):3–44, 2002.
- 345 12. H Schnack-Petersen, Ragnar Bengtsson, RA Bark, P Bosetti, A Brockstedt, H Carlsson, LP Ek-  
346 ström, GB Hagemann, B Herskind, F Ingebretsen, et al. *Nuclear Physics A*, 594(2):175–202,  
347 1995.
- 348 13. S Biswas, R Palit, S Frauendorf, U Garg, W Li, GH Bhat, JA Sheikh, J Sethi, S Saha, Purnima  
349 Singh, et al. *The European Physical Journal A*, 55(9):1–7, 2019.
- 350 14. James Till Matta. Transverse wobbling in 135 pr. In *Exotic Nuclear Excitations: The Transverse*  
351 *Wobbling Mode in 135 Pr*, pages 77–93. Springer, 2017.
- 352 15. N Sensharma, U Garg, S Zhu, AD Ayangeakaa, S Frauendorf, W Li, GH Bhat, JA Sheikh, MP Car-  
353 penter, QB Chen, et al. *Physics Letters B*, 792:170–174, 2019.

16. S Chakraborty, HP Sharma, SS Tiwary, C Majumder, AK Gupta, P Banerjee, S Ganguly, S Rai, S Kumar, A Kumar, et al. *Physics Letters B*, 811:135854, 2020.
17. J Timár, QB Chen, B Kruzsicz, D Sohler, I Kuti, SQ Zhang, J Meng, P Joshi, R Wadsworth, K Starosta, et al. *Physical review letters*, 122(6):062501, 2019.
18. S Nandi, G Mukherjee, QB Chen, S Frauendorf, R Banik, Soumik Bhattacharya, Shabir Dar, S Bhattacharyya, C Bhattacharya, S Chatterjee, et al. *Physical Review Letters*, 125(13):132501, 2020.
19. N Sensharma, U Garg, QB Chen, S Frauendorf, DP Burdette, JL Cozzi, KB Howard, S Zhu, MP Carpenter, P Copp, et al. *Physical review letters*, 124(5):052501, 2020.
20. JH Hamilton, SJ Zhu, YX Luo, AV Ramayya, S Frauendorf, JO Rasmussen, JK Hwang, SH Liu, GM Ter-Akopian, AV Daniel, et al. *Nuclear Physics A*, 834(1-4):28c–31c, 2010.
21. YX Luo, JH Hamilton, AV Ramaya, JK Hwang, SH Liu, JO Rasmussen, S Frauendorf, GM Ter-Akopian, AV Daniel, Yu Ts Oganessian, et al. Triaxial and triaxial softness in neutron rich ru and pd nuclei. In *Exotic Nuclei: EXON-2012*, pages 215–224. World Scientific, 2013.
22. CM Petrache, PM Walker, S Guo, QB Chen, S Frauendorf, YX Liu, RA Wyss, D Mengoni, YH Qiang, A Astier, et al. *Physics Letters B*, 795:241–247, 2019.
23. YK Wang, FQ Chen, and PW Zhao. *Physics Letters B*, 802:135246, 2020.
24. QB Chen, S Frauendorf, and CM Petrache. *Physical Review C*, 100(6):061301, 2019.
25. S Frauendorf and F Döna. *Physical Review C*, 89(1):014322, 2014.
26. Ikuko Hamamoto. *Physical Review C*, 65(4):044305, 2002.
27. Kosai Tanabe and Kazuko Sugawara-Tanabe. *Physical Review C*, 73(3):034305, 2006.
28. AS Davydov and GF Filippov. *Nuclear Physics*, 8:237–249, 1958.
29. AA Raduta, R Poenaru, and L Gr Ixaru. *Physical Review C*, 96(5):054320, 2017.
30. AA Raduta, CM Raduta, and R Poenaru. *Journal of Physics G: Nuclear and Particle Physics*, 48(1):015106, 2020.
31. AA Raduta, R Budaca, and CM Raduta. *Physical Review C*, 76(6):064309, 2007.
32. AA Raduta, R Poenaru, and AI H Raduta. *Journal of Physics G: Nuclear and Particle Physics*, 45(10):105104, 2018.
33. R Budaca. *Physical Review C*, 97(2):024302, 2018.
34. AA Raduta, R Poenaru, and CM Raduta. *Physical Review C*, 101(1):014302, 2020.
35. DR Jensen, GB Hagemann, I Hamamoto, B Herskind, G Sletten, JN Wilson, SW Ødegård, K Spohr, H Hübel, P Bringel, et al. *The European Physical Journal A-Hadrons and Nuclei*, 19(2):173–185, 2004.
36. J Meyer-ter Vehn. *Nuclear Physics A*, 249(1):111–140, 1975.
37. SY Wang, SQ Zhang, B Qi, J Peng, JM Yao, J Meng, et al. *Physical Review C*, 77(3):034314, 2008.
38. EA Lawrie, O Shirinda, and CM Petrache. *Physical Review C*, 101(3):034306, 2020.